RESEARCH ARTICLE

Key Points:
- Model resolution-dependent changes in Atlantic Ocean heat transport and surface heat fluxes are determined using three climate models
- Increasing ocean resolution to eddy-permitting raises Atlantic heat transport; changing atmospheric resolution only impacts surface fluxes
- Enhancing ocean resolution to eddy-resolving results in a further increase in Atlantic Heat Transport and the best observational agreement

Correspondence to:
J. P. Grist,
jeremy.grist@noc.ac.uk

Increasing Atlantic Ocean Heat Transport in the Latest Generation Coupled Ocean-Atmosphere Models: The Role of Air-Sea Interaction

Jeremy P. Grist[1] [iD], Simon A. Josey[1] [iD], Adrian L. New[1], Malcolm Roberts[2] [iD], Torben Koenigk[3] [iD], and Doroteaciro Iovino[4]

[1]National Oceanography Centre, European Way, Southampton, SO14 3ZH, UK, [2]Met Office, Exeter, UK, [3]SMHI, Norrköping, Sweden, [4]Fondazione Centro Euro-Mediterraneo sui Cambiamenti Climatici, Bologna, Italy

Abstract Recent increases in resolution of coupled ocean-atmosphere models have the potential to improve the representation of poleward heat transport within the climate system. Here we examine the interplay between model resolution-dependent changes in Atlantic Ocean heat transport (AOHT) and surface heat fluxes. The different roles of changes in atmospheric and ocean resolution are isolated using three different climate models (The Centro Euro-Mediterraneo sui Cambiamenti Climatici Climate Model 2, Hadley Centre Global Environmental Model 3 – Global Coupled configuration 2, and European Community Earth-System Model 3.1) and comparing runs in which (a) only the ocean resolution changes, (b) only the atmosphere resolution changes, and (c) both change. Enhancing ocean resolution from eddy parameterized to eddy permitting increases the AOHT throughout the basin, values changing from 1.0 to 1.2 PW at 26°N, bringing the AOHT into the range of estimates from the RAPID observing array. This increase in AOHT is associated with higher North Atlantic sea surface temperatures and increased ocean heat loss to the atmosphere. Increasing the atmospheric resolution alone has little impact on the AOHT due to regionally compensating changes in the components of the net heat flux. Finally, in a fourth experiment the impact of resolution changes in both components and the transition to an eddy-resolving ocean is assessed. This additional resolution increase is accompanied by a further change in the AOHT and improves agreement with observations in the tropics but not the subpolar regions. However, unlike with the increase to the eddy-permitting ocean, when the greatest AOHT change occurs in the subtropics and subpolar region, the most significant increase now occurs in the tropics.

Plain Language Summary The ocean and atmosphere export large amounts of heat from the tropics toward more poleward latitudes. In the Northern Hemisphere about 25% of this export is accomplished by the movement of water in the Atlantic Ocean. It is therefore important for climate models to accurately simulate this *Atlantic Ocean heat transport* (AOHT). However, historically climate models have typically underestimated AOHT relative to our best observations. This paper investigates how changing the size of the grid cells in the model changes both AOHT and the ocean-to-atmosphere exchange of heat in the model. Reducing the size of the grid cells in the models is referred to as increasing the resolution. Increasing the resolution of the ocean component of the model to 1/4° latitude and longitude increases AOHT, making agreement with observations better in the subtropics but slightly worse in subpolar regions. Increasing the resolution of the atmospheric part of the model had little effect on AOHT, instead bringing changes to different parts of the ocean-to-atmosphere heat exchange that compensate each other. Finally, we examined the AOHT in one of the newest climate models with even higher resolution (1/12° ocean and 25-km atmosphere). Additional improvements in the simulation of AOHT were found.

1. Introduction

The meridional Atlantic Ocean heat transport (hereafter AOHT) is a fundamental aspect of the climate system that climate models have found difficult to accurately represent. Observations show that the AOHT peaks at about 1.25 (±0.36) PW (Johns et al., 2011; McCarthy et al., 2015) at 26°N, which represents about 20–25% of estimates for the total (global ocean and atmosphere) export of heat from the tropics to the northern latitudes (Trenberth & Caron, 2001). Large regional changes in ocean heat content have been attributed to AOHT variability; for example, the strong Atlantic subpolar gyre warming of the mid-1990s (Grist et al., 2010) although surface fluxes can also play a significant role (Grist et al., 2016; Josey et al., 2018). In addition,

Table 1
Details of Model Experiments Conducted in the Study

| Experiment	Model	High resolution	Low resolution
1. Ocean-only (HRo-LRo) present-day forcing control run	CMCC CM2 (Fogli & Iovino, 2014)	Abbreviation: HRo Atmosphere: 192 × 288 (~100 × 140 km) Ocean: ORCA025 (1/4°) Run length: 39 years	Abbreviation: LRo Atmosphere: 192 × 288 (~100 × 140 km) Ocean: ORCA1 (1°) Run length: 300 years
2. Atmosphere only (HRa-LRa) present-day forcing control run	HadGEM3 GC2.0 (Williams et al., 2015)	Abbreviation: HRa Atmosphere: N512 (~25 km) Ocean: ORCA025 (1/4°) Run length: 97 years	Abbreviation: LRa Atmosphere: N96 (~135 km) Ocean: ORCA025 (1/4°) Run length: 99 years
3. Atmosphere and ocean (HRoa-LRoa) historical forcing from 1950 (LRoa) and 1990 (HRoa)	EC EARTH 3.1 (Hazeleger et al., 2012, Sterl et al., 2012)	Abbreviation: HRoa Atmosphere: T511 (~40 km) Ocean: ORCA025 (1/4°) Run length: 25 years	Abbreviation: LRoa Atmosphere: T255 (~80 km) Ocean: ORCA1 (1°) Run length: 60 years
4. CMIP6 (VHRoa-HRoa2)	HadGEM3 GC2.1 (Hewitt et al., 2016)	Abbreviation: VHRoa Atmosphere: N512 (~25 km) Ocean: ORCA12 (1/12°) Run length: 20 years	Abbreviation: HRoa2 Atmosphere: N216 (~60 km) Ocean: ORCA025 (1/4°) Run length: 20 years

Note. CMIP = Coupled Model Intercomparison Project Phase 6.

Atlantic Ocean temperatures have the potential to modulate both winter and summer European climate (Buchan et al., 2014; Maidens et al., 2013; Pohlmann et al., 2006; Sutton & Hodson, 2005).

Historically, observational estimates of the AOHT were based on transatlantic hydrographic sections (Bryden & Hall, 1980). By their nature, these observations were limited to specific times and latitudes. Since 2004, continuous estimates have been made by the RAPID dedicated observing array at 26°N, near the latitude of maximum northward transport (Cunningham et al., 2007; McCarthy et al., 2015). The array measurements have demonstrated significant seasonal variability in the Atlantic Meridional Overturning Circulation (AMOC) and the AOHT with which it is highly correlated (Johns et al., 2011). The seasonal AMOC amplitude at 26°N is greater than 6 Sv and can complicate the interpretation of earlier sporadic measurements; in particular, a trend found from five repeat hydrographic sections over a period of order 40 years (Bryden et al., 2005) virtually disappeared when the individual sections were corrected for their seasonal bias (Kanzow et al., 2010).

The midlatitudes and the subpolar gyre have also been the focus of attempts to produce continuous basin-integrated estimates of AOHT. At 41°N, the vertical density structure determined from Argo floats has been combined with satellite-based sea surface height estimates to produce monthly estimates of AOHT from 2002 onward (Hobbs & Willis, 2012). In addition, a section between Canada (53°N), Greenland (60°N), and Scotland (56°N) occupied in 2014 and 2016 (Holliday et al., 2018) is now the focus of the dedicated observing array of the *Overturning in the Subpolar North Atlantic Program* (OSNAP). OSNAP aims to provide subseasonal estimates of ocean heat transport as one of its main objectives (Lozier et al., 2017).

Whereas the aforementioned observations are associated with estimates at specific sections, Trenberth and Fasullo (2017) have detailed an observation-based method of producing continuous estimates of AOHT over a range of latitudes. In their approach top-of-atmosphere radiation is combined with atmospheric reanalysis to estimate surface heat fluxes. The surface heat fluxes were then combined with vertically integrated ocean heat content to calculate AOHT as a residual. The resulting times series consists of monthly estimates from 2000 to 2014 between 30°S and 60°N. The estimates produced good temporal agreement with the 26°N RAPID array, although the mean value was about 0.2 PW weaker.
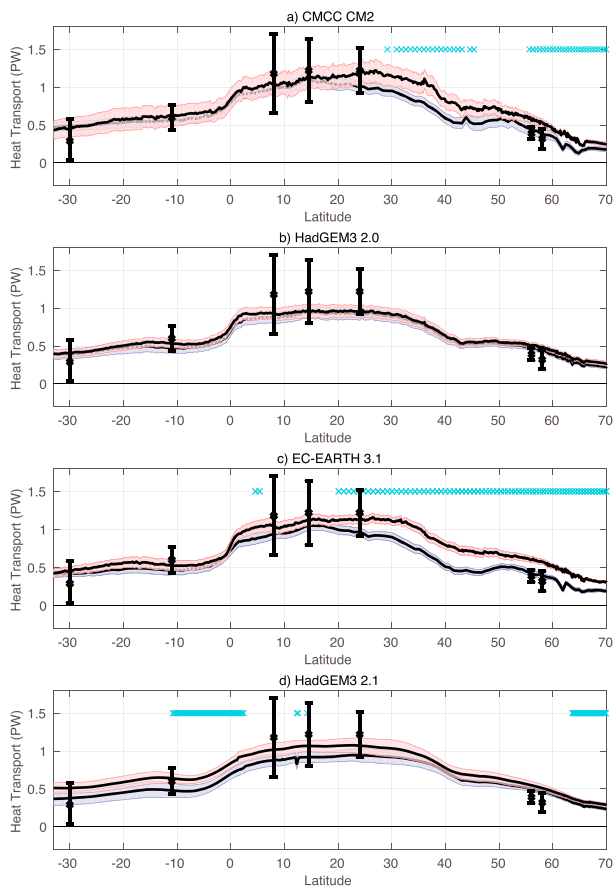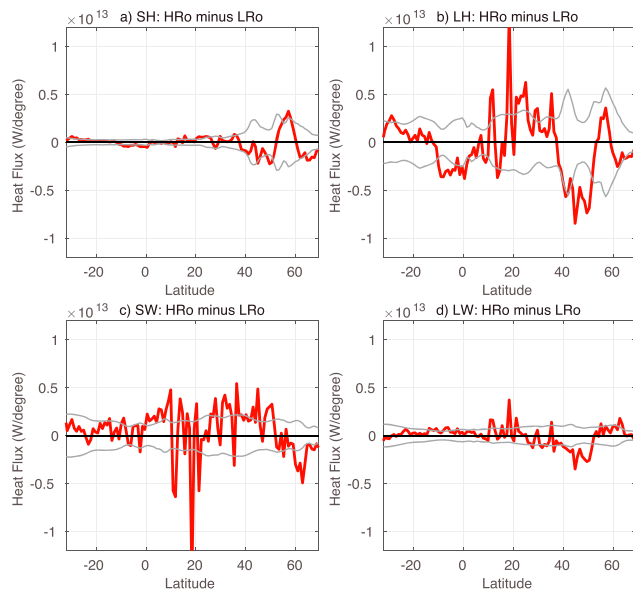
Figure 1. Annual mean zonally integrated meridional Atlantic Ocean heat transport (unit: PW) for experiments (a) 1, (b) 2, (c) 3, and (d) 4. Red lines indicate higher resolution. Blue lines indicate lower resolution. Shading indicates interannual standard deviations. Black error bars indicate observational estimates from hydrographic sections Holliday et al. (2018; 2014 and 2016 estimates near 56°N), Lavin et al. (1998; 26°N), Klein et al. (1995; 14°N), Klein et al. (1995; 8°N), Speer et al. (1996; 11°S), and Holfort and Siedler (2001; 30°S). (a) HRo and LRo, (b) HRa and LRa, (c) HRoa and LRoa, and (d) VHRoa and HRoa2. The cyan crosses indicate latitudes where the model Atlantic Ocean heat transport values do not fall within each other's standard deviations.

Despite the climatic importance of the Atlantic heat transport and the significant recent progress in characterizing its mean and variability in space and time, it is still poorly reproduced in climate models that generally underestimate its magnitude (Jia, 2003; Msadek et al., 2013). However, recently, as the model resolution has increased, the modeled AOHT has reached better agreement with observations (Kirtman et al., 2012; Roberts et al., 2016). An important climate impact of a change in model AOHT (or more specifically the meridional convergence of AOHT), whether it arises from a resolution change or another process, is that it is accompanied by a change in the net air-sea heat flux. At present, the mechanisms linking the AOHT and surface flux changes (in particular which components of the heat flux change and in what regions) are not well understood. For example, Roberts et al. (2016) compared a high-resolution (25-km atmosphere, 1/12° eddy-resolving ocean) to a lower-resolution (60-km atmosphere, 1/4° eddy-permitting ocean) configuration of Hadley Centre Global Environmental Model 3 – Global Coupled configuration 2.1, (HadGEM3-GC2.1). They found a significant increase in midlatitude latent heat loss from the ocean that was associated with an increase in sea surface temperature (SST). In an earlier study, Kirtman et al. (2012) investigated the impact of small-scale oceanic features on the modeled large-scale climate, comparing versions of the National Center for Atmospheric Research Community Climate System Model 3.5, having the same resolution in the atmosphere ($0.625° \times 0.5°$) but changing from eddy permitting to eddy resolving in the ocean. They also found the higher-resolution model had greater global ocean heat transport and higher SSTs in regions of strong eddy activity. However, in their analysis changes in shortwave radiation were a particularly important component of the changes in the surface heat flux. Thus, the resolution-dependent mechanisms by which the ocean heat transport and air-sea energy exchanges are linked remain to be robustly determined.

In order to improve our understanding of the impact of increased resolution in both atmospheric and ocean components on AOHT and the link to surface heat flux processes, we analyze experiments with three different climate models that have been run at varying resolutions (full model details are given in section 2). In the first experiment, with the The Centro Euro-Mediterraneo sui Cambiamenti Climatici Climate Model 2 (CMCC CM2) the 1° atmosphere resolution is held constant and coupled to different ocean meshes, an eddy-parameterizing (ORCA1, 1°) and an
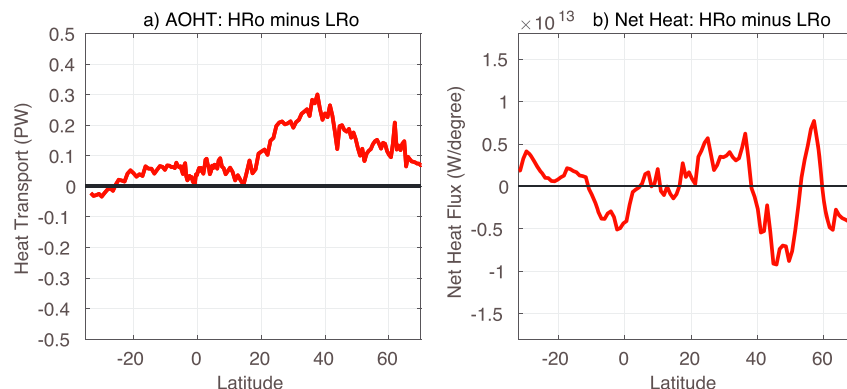
Figure 2. HRo-LRo difference in (a) annual mean AOHT (PW) and (b) zonally integrated net surface heat flux for the Atlantic basin (unit: W per degree latitude). AOHT = Atlantic Ocean heat transport.

Figure 3. Annual mean HRo-LRo difference in the zonally integrated surface heat flux components for the Atlantic basin (unit: W per degree latitude): (a) sensible heat flux, (b) latent heat flux, (c) shortwave, and (d) longwave. Gray lines indicate ± the LRo interannual standard deviation.
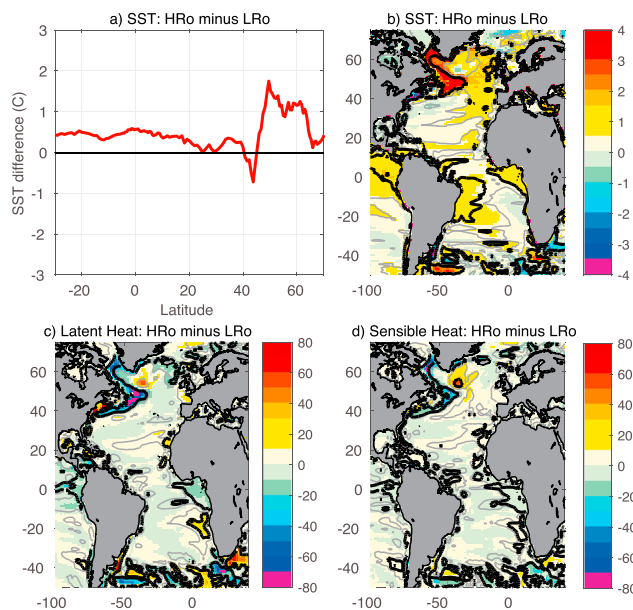
Figure 4. (a) Annual mean HRo-LRo difference in zonally integrated SST for the Atlantic basin (°C). Annual mean HRo-LRo difference for (b) SST (°C). (c) Air-sea latent heat flux (W/m²). (d) Air-sea sensible heat flux (W/m²). Gray and black contours are one and two standard deviations of LRo, respectively. SST = sea surface temperature.

eddy permitting (ORCA025, 1/4°) configuration. In the second experiment, the climate model is HadGEM3 GC2.0 and has an eddy-permitting ocean (ORCA025, 1/4°) that is unchanged but an atmosphere that increases resolution from 130 to 25 km. In the third experiment, with European Community Earth-System Model 3.1 (EC-EARTH 3.1), there are increases in both the atmosphere (from 80 to 40 km) and ocean (from non eddy-permitting, ORCA1 to eddy permitting, ORCA025) resolutions. Although the three models used are a small cross section of Intergovernmental Panel on Climate Change (IPCC) class models, the experiment design allows us to both isolate and combine, the role of ocean and atmospheric resolutions. The approach also allows us to develop a framework for understanding the impact of resolution changes in current and future versions of climate models. To this end, we also examine a pair of short runs from a model developed for the forthcoming High Resolution Intercomparison Project (Haarsma et al., 2016) in the framework of the Coupled Model Intercomparison Project Phase 6 (CMIP6) exercise in which the ocean resolution is further increased to explicitly resolve eddies in most of the global basin and the atmosphere resolution increases up to 25 km.

The structure of this paper is as follows. In section 2, we describe the experimental design and climate models used for the analysis. In section 3, the results from the three pairs of noneddy-permitting and eddy-permitting models are presented in turn. Then in section 4, results of the change from the eddy-permitting to eddy-resolving model are presented. In the final section, we develop a conceptual framework for the resolution-dependent changes in AOHT and surface heat fluxes and summarize the key results.

2. Models and Methods

Numerical experiments based on three global coupled ocean-atmosphere model experiments are reported here. The experiments consist of pairs of runs within which the model remains the same, but the resolution for (a) ocean only, (b) atmosphere only, and (c) both atmosphere and ocean is changed. A summary of the model runs that make up these experiments is included in Table 1. All these models are global coupled climate General Circulation Models (including the atmosphere, ocean, and sea ice components). They all share the Nucleus for European Modelling of the Ocean (NEMO) ocean model (Madec, 2008) in either the ORCA1 or ORCA025 configuration. These configurations have resolutions of 1° and 1/4°, respectively at the equator, with meshes that become finer at higher latitudes.

Experiment 1, which is referred to as the *ocean-only case*, uses the CMCC-CM2 model (Fogli & Iovino, 2014) with unchanged atmospheric resolution of 0.94° latitude by 1.25° longitude and two different resolutions of the tripolar ocean meshes: the low-resolution (LRo) configuration corresponds to a 1° horizontal resolution (ORCA1, with a tropical refinement of the meridional spacing down to a ~1/3°) and the high-resolution version (HRo) to a 1/4° configuration (ORCA025). Both LRo and HRo are initiated from the end state of an over 100-year simulation of the LRo. For LRo additional spin-up is included in the averaging period/run length (Table 1), while HRo had a multidecade spin-up. For experiment 2, which is referred to as the *atmosphere-only* case, we use the HadGEM3 GC2.0 model (Williams et al., 2015) with the low-resolution (LRa) being an N96 (approximately 135 km) atmosphere and a 1/4° ocean (ORCA025) and
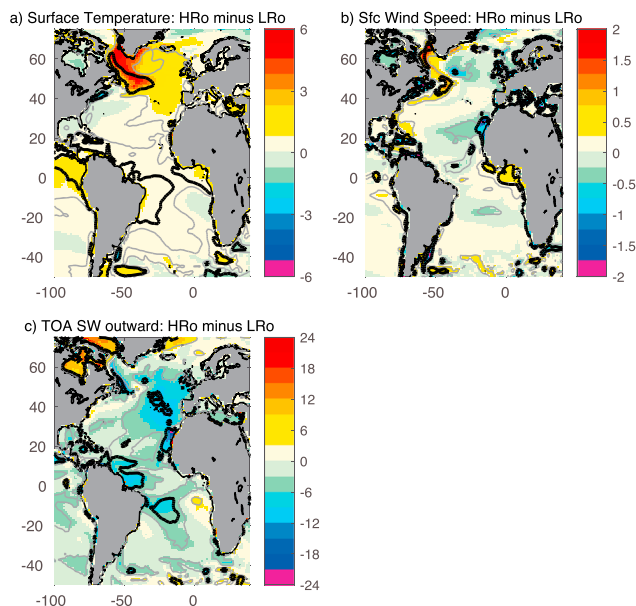
Figure 5. Annual mean HRo-LRo difference: (a) ocean surface air temperature (°C), (b) ocean surface wind speed (m/s), and (c) TOA outgoing shortwave radiation (W/m^2) over the ocean. Gray and black contours are one and two standard deviations of LRo, respectively. TOA = top of atmosphere.

the high-resolution version (HRa) being an N512 (approximately 25 km) atmosphere with the same 1/4° ocean (ORCA025). The models are initiated from the EN3 (Ingleby & Huddleston, 2007) observational temperature-salinity climatology and with constant present-day (year 2000) greenhouse forcing. The spin-up is included in the averaging period/run length (Table 1). As indicated in Williams et al. (2017), the model surface climatology takes around 30 years to reach a pseudo-equilibrium, with a top-of-atmosphere radiative imbalance of about 0.6 W/m^2, which is consistent with present-day forcing. The adjustment timescale for the deeper ocean is clearly longer, with the largest global-mean ocean temperature drift (0.11 K/decade[1]) occurring at 563 m. However, the HRa minus LRa AOHT difference remains stable over the course of the run, indicating that both models adjust in similar ways.

Experiment 3, which is referred to as the *ocean-atmosphere case*, uses the Climate Model EC-EARTH3.1 with the low-resolution (LRoa) being a T255 (~80 km) atmosphere (91 Levels) and a 1° ocean (ORCA1), and the high-resolution version (HRoa) is T511 (~40 km) atmosphere (91 Levels) and 1/4° ocean (ORCA025). EC-Earth3.1 is a successor of the CMIP5 version, EC-Earth2.3 (Hazeleger et al., 2012; Sterl et al., 2012), and uses updated versions of its atmosphere (Integrated Forecasting System-IFS, cycle36r4) and ocean (NEMO3.3.1), as used by Koenigk and Brodeau (2017). The LRoa simulation started from an EC-Earth3.01 historical simulation in 1950. This historical simulation with EC-Earth3.01 used CMIP5-forcing and started from a 500-year Pre Industrial-control simulation. EC-Earth31 differs from EC-Earth3.01 mainly in technical updates, in the resolving of a few bugs, particularly in the output of sea ice variables and in a slight update of the ORCA1 ocean bathymetry. For HRoa a 44-year spin-up has been performed with constant averaged 1955–1965 forcing. The historical high-resolution simulation started from this spin-up using CMIP5 forcing in 1960. In this study, the later part of this simulation, 1990–2015, is used as HRoa.

The experiments are analyzed by examining the differences between the high- and low-resolution configurations in key mean quantities such as heat transport, heat flux components, SST, air temperature, and wind speed. Unless otherwise noted, high resolution-low resolution difference will be referred to as significant if the difference exceeds the interannual standard deviation of the low-resolution run. On spatial maps multiples of the standards deviations are plotted as contours. The goal of the approach is to identify the relative sensitivity of the AOHT changes to ocean and atmospheric resolution and to establish the key surface flux processes that balance these changes.

We then examine AOHT and surface flux changes in a model configuration with even finer resolution, to consider if the same findings are likely to hold as climate model resolution moves beyond that which will be typical of the CMIP6 exercise. Specifically in Experiment 4, a version of HadGEM3-GC2.1 (Hewitt et al., 2016) with an N512 atmosphere and a 1/12° (ORCA12) eddy-resolving ocean (referred to as VHRoa) is compared with a lower-resolution version that has an N216 atmosphere and a 1/4° (ORCA025) ocean (referred to as HRoa2). The initial conditions and forcing are the same as used for HadGEM3-GC2.0. These simulation are only 20 years in length and hence not yet in near-surface quasi-equilibrium. However, as shown in Roberts et al. (2016) the VHRoa model mean state is outside the variability from a longer HadGEM3-GC2 simulation, and the top-of-atmosphere flux balance was little changed between HadGEM3-GC2.0 and HadGEM3-GC2.1. In addition, more recent coupled HadGEM3-GC3.1 N216-ORCA12 simulations following the High Resolution Intercomparison Project experimental design (Haarsma et al., 2016) of 150 years in length indicate that the AOHT remains fairly stable after 20–30 years of spin-up. Finally, we note that the ocean resolution of HRoa2 in Experiment 4 is comparable to
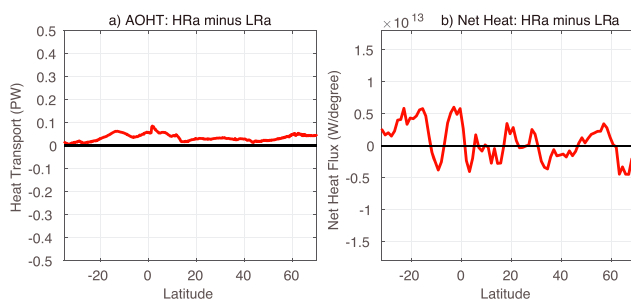
Figure 6. HRa-LRa difference in (a) annual mean AOHT (PW) and (b) zonally integrated net heat flux for the Atlantic basin (unit: W per degree latitude). AOHT = Atlantic Ocean heat transport.
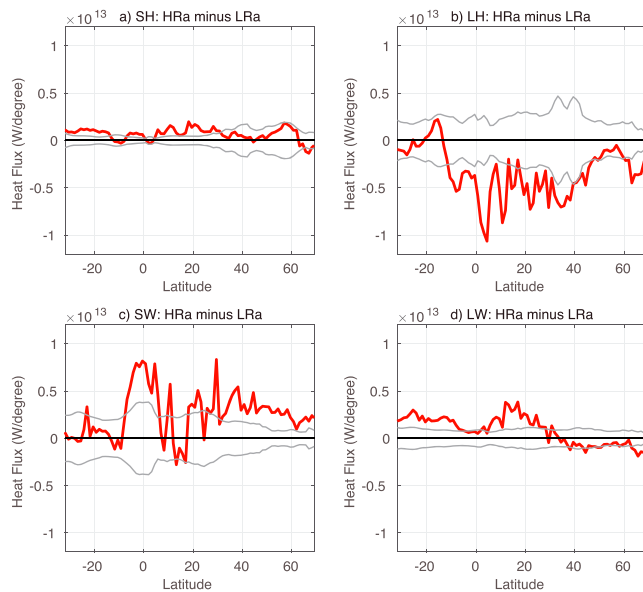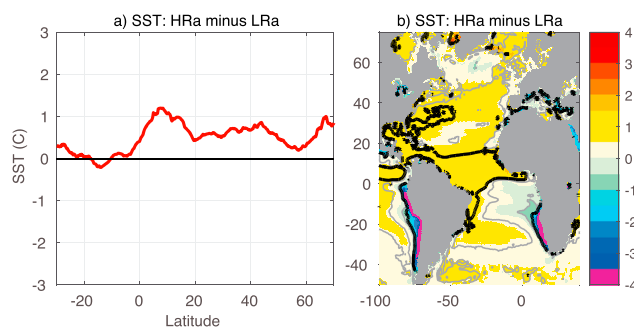
Figure 7. Annual mean HRa-LRa difference in the zonally integrated heat flux components for the Atlantic basin (unit: W per degree latitude): (a) sensible heat flux, (b) latent heat flux, (c) shortwave, and (d) longwave. Gray lines indicate ± the LRa interannual standard deviation.

Figure 8. (a) Annual mean HRa-LRa difference in zonally integrated SST for the Atlantic basin (°C) and (b) annual mean HRa-LRa SST (°C) difference. Gray and black contours are one and two standard deviations of LRa, respectively. SST = sea surface temperature.

that in higher-resolution runs in Experiments 1–3 and the atmospheric resolution is comparable with that in Experiments 2 and 3.

3. Model Results: 1° to 1/4° Ocean

3.1. Experiment 1: Ocean-Only Resolution Changing

We first examine the ocean-only case using the CMCC simulations. The AOHT for both the HRo and the LRo cases is displayed as a function of latitude in Figure 1a, while the HRo-LRo AOHT difference is in Figure 2a. The HRo has increased AOHT throughout the Atlantic basin relative to the LRo version. Between 20°N and 62°N the difference is greater than 0.1 PW, with a peak 0.3 PW difference at 38°N. This difference increases notably between 20°N and 38°N, declines markedly between approximately 38°N and 50°N, then increases slightly between 50°N and 60°N, before declining again further north. The sense of these changes is that it brings the model AOHT into closer agreement with observations in the North Atlantic subtropics but further away from observations in the subpolar regions. In the Southern Hemisphere the HRo-LRo difference is positive north of 25°S but less than 0.1 PW.

The HRo-LRo difference in the zonally integrated net heat flux (Figure 2b, using the convention that positive values represent heat flux into the ocean) presents a more complex change with latitudes. However, a key feature is the increase in ocean heat loss between 38°N and 50°N, with a smaller increase in heat gain between 50°N and 60°N, and a further loss north of 60°N. These features, together with the increase in heat gain between 20°N and 38°N, are consistent with the features in the AOHT difference (Figure 2a). Note that a priori the latitude-integrated changes in surface heat flux would not be expected to exactly match the difference in diagnosed AOHT as the model may contain variations in the ocean heat storage terms (i.e., which might result from the model not being in thermal equilibrium). However, the small temporal variability of the AOHT in each model indicates that the ocean heat content changes were also small. For example, the CMCC LRo run has AOHT values at 26°N of 0.97 PW (with an annual standard deviation of 0.07 PW) for years 1–150 and 1.00 PW (with an annual standard deviation of 0.07 PW) for years 151–300. The stable values of AOHT are consistent with the good agreement between the patterns in Figures 2a and 2b and indicate that variations in ocean heat storage are small. We will now consider in more detail the individual flux components.

The zonally integrated components of the net heat for HRo-LRo are shown in Figure 3. In the sign convention used here, a positive heat flux acts to warm the ocean. Thus, latent heat flux is predominantly negative (cooling the ocean) and shortwave is positive (warming the ocean). A large part of the net heat flux difference is distinctly associated with changes in the latent heat flux (Figure 3b). Concentrating on the latitude bands where there are significant HRo-LRo differences, it is noted that there is generally a significant decrease in ocean latent heat loss between 15°N and 38°N and some significant increases in latent heat loss between 10°S and 10°N and between 38°N and 52°N. In this latter region, the increased loss is supported by a significant increased loss from the flux of longwave radiation (Figure 3d). There is a significant increase in incoming shortwave radiation (~3.0–5.0 × 10^{12} W) between the equator and 10°N and between 30°N and 50°N. There is also a reduction in incoming shortwave radiation near 60°N as well as some spikes of reduced shortwave near 10°N and 20°N. These spikes in reduced shortwave appear to be reflected in spikes in reduced flux of latent heat to the atmosphere (Figure 3b).
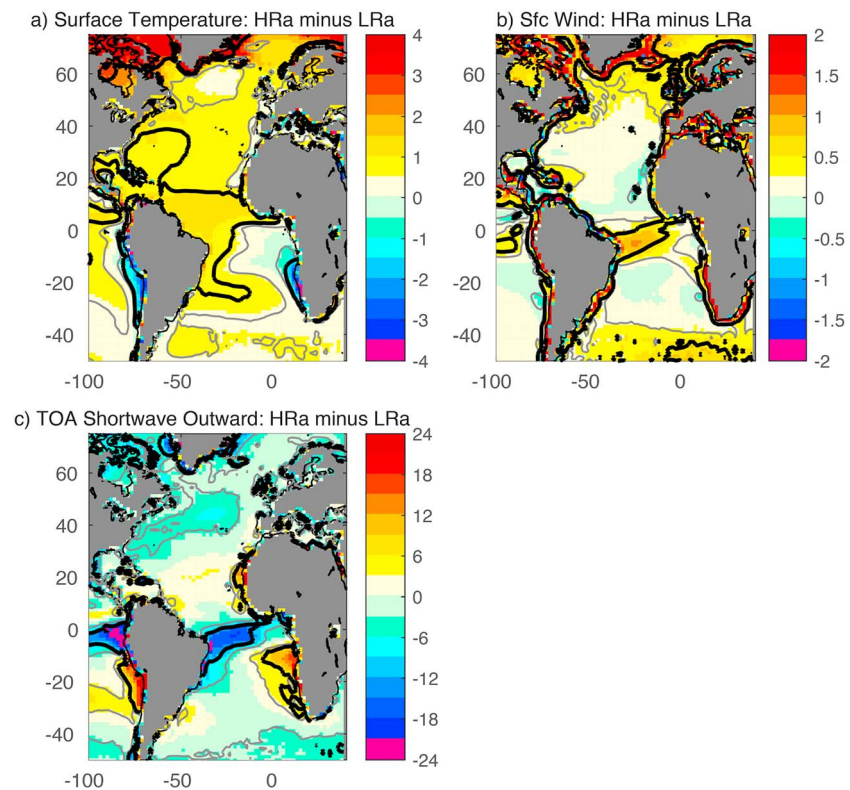
Figure 9. Annual mean HRa-LRa difference: (a) ocean surface air temperature (°C), (b) ocean surface wind speed (m/s), and (c) TOA outgoing shortwave radiation over the ocean (W/m^2). Gray and black contours are one and two standard deviations of LRa, respectively. TOA = top of atmosphere.

Summarizing the effect of enhanced resolution in the ocean-only case, it is noted first that higher resolution results in a significant increase in AOHT; in particular, between 20°N and 62°N the difference is greater than 0.1 PW, which is a significant fraction of the total. The AOHT difference broadly rises between 20°N and 38°N (peaking at 0.3 PW) and reduces further to the north. These differences are closely in line with expectations from the differences in the net ocean-atmosphere heat flux differences. In turn, the accompanying changes in the net heat flux terms are dominated by changes in latent heat flux and modulated somewhat by shortwave changes.

Table 2

Annual Mean (and Standard Deviation) of the 26°N AOHT (PW) by Ocean and Atmosphere Resolution for All the Model Integrations

Atmosphere resolution	Ocean resolution		
	1°	1/4°	1/12°
100 × 140 km (LRo)	0.98 (±0.07)		
80 km (LRoa)	0.92 (±0.05)		
100 × 140 km (HRo)		1.20 (±0.14)	
135 km (LRa)		0.92 (±0.08)	
60 km (HRoa2)		0.94 (0.09)	
40 km (HRoa)		1.16 (±0.06)	
25 km (HRa)		0.95 (±0.08)	
25 km (VHRoa)			1.06 (±0.11)

Note. AOHT = Atlantic Ocean heat transport.

The zonally integrated HRo-LRo SST difference is plotted in Figure 4a. It shows an increase in SST (>1 °C) between 50°N and 62°N. The spatial pattern of higher SST is consistent with increased latent, sensible, and longwave loss to the atmosphere (Figure 4b). The SST increase in the North Atlantic (Figure 4b) is particularly pronounced on the western side of the subpolar gyre. This increase has two main centers: one, at 50°N and 20°W, is consistent with a stronger eastward extension of the North Atlantic Current (NAC) and the second, adjacent to the Labrador and Greenland Coast, is likely related to a reduction in Arctic sea ice exposing the warmer underlying ocean surface. Detailed analysis, beyond the scope of this study, is required to fully identify and separate the effects of these two processes. Furthermore, there is an area near 55°N characterized by a slight reduction in SST. This is consistent with a reduction in latent and sensible heat loss to the atmosphere in the same region (Figures 4c and 4d).

We now consider in Figure 5 changes in the atmospheric fields with a focus on the Atlantic Sector. First, the change in surface air

Table 3
Annual Mean (and Standard Deviation) of the 40°N AOHT (PW) by Ocean and Atmosphere Resolution for All the Model Integrations

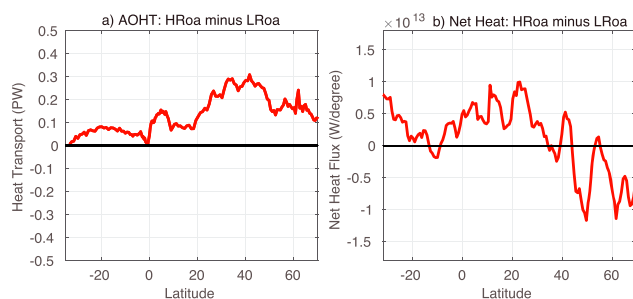| Atmosphere resolution	Ocean resolution		
	1°	1/4°	1/12°
100 × 140 km (LRo)	0.59 (±0.07)		
80 km (LRoa)	0.55 (±0.04)		
100 × 140 km (HRo)		0.82 (±0.11)	
135 km (LRa)		0.60 (±0.06)	
60 km (HRoa2)		0.72 (±0.07)	
40 km (HRoa)		0.80 (±0.05)	
25 km (HRa)		0.63 (±0.06)	
25 km (VHRoa)			0.77 (±0.07)

Note. AOHT = Atlantic Ocean heat transport.

temperature shows warming over the subpolar North Atlantic Ocean. This difference is consistent with increased ocean heat loss warming the atmosphere as opposed to the atmospheric changes influencing the ocean (Figure 5a). However, because of the coupled nature of surface flux processes, it cannot be ruled out that some of the ocean-initiated changes in the atmosphere feed back on to the ocean. For example, the significant changes in surface wind over the North Atlantic subpolar gyre (Figure 5b) are in the correct sense to promote the changes in turbulent fluxes seen in Figures 4c and 4d. Specifically, the increased wind speed on the western perimeter of the Labrador Sea would have promoted the increased sensible and latent heat loss. Another example of changes in the surface wind potentially influencing the turbulent fluxes is in the central subpolar gyre. As mentioned previously the central subpolar gyre is characterized by a weak decrease in SST and a strong decrease in turbulent fluxes. Figure 5b also shows that this is an area of decreased wind speed, promoting

the decrease in turbulent fluxes. The exact coupled mechanism whereby a change in the ocean transport could lead to a decrease in wind speed that effectively suppresses the turbulent heat loss is not clear, although it is possible that a more northerly ice edge in the high heat transport run could lead to a northward shift of the surface temperature gradients. Finally, in terms of atmospheric changes in the ocean-only case, we consider the changes in outward shortwave radiation at the top of the atmosphere (TOA) in Figure 5c. There are significant reductions in cloud cover in the eastern midlatitude Atlantic and over the western Labrador Sea, so that less shortwave is reflected outward in these regions. There are also local differences in the Caribbean Sea and off the West African Coast. These lead to the short spatial scale variability seen in the zonally integrated shortwave plots (Figure 3). Again, the fact that there are significant changes in this atmospheric field suggests that changes in ocean resolution are causing important changes to the atmospheric circulation and properties.

Summarizing the ocean-only case, it is evident that increasing the resolution from LRo to HRo implies a significant increase in northward ocean heat transport in the North Atlantic. This is balanced primarily by an increase in mid-high latitude latent heat loss. The increased latent heat loss is driven by the ocean resolution change, being associated with increased SSTs and reduced sea ice coverage.

3.2. Experiment 2: Atmospheric-Only Resolution Changing

We now consider the atmosphere-only case using HadGEM3-GC2 models with a higher-resolution grid only in the atmospheric component. The AOHT for both high (HRa) and low (LRa) resolution is shown in Figure 1b, and the HRa-LRa difference is shown in Figure 6a. The change in atmospheric resolution does not bring about a significant change in the AOHT, implying that it is the increase in ocean resolution to at least 1/4° that is most important to improve the AOHT compared with observation-based estimates (see Figure 1a). The relatively small (<0.1 PW) changes in AOHT in Figure 6a are reflected in values of the HRa-LRa zonally integrated net heat flux that fluctuate around zero by small (<0.7 × 10^{13} W per degree latitude) amounts (Figure 6b).

The relatively small changes in net heat flux disguise the fact that there are significant changes in the latent and shortwave individual components that compensate each other. The zonally integrated values for the four components of the heat flux are shown in Figure 7 and present a significant increase in ocean latent heat loss (>~0.2 × 10^{13} W per degree latitude) between 10°S and 45°N (Figure 7b). There is also an increase in shortwave flux into the ocean at all latitudes north of 8°S with the exception of a small subregion between 5°N and 25°N (Figure 7c).

We now examine the fields that could drive changes in the component fluxes in Figure 8. The HRa-LRa SST is typically 0.5–1.0 °C warmer than LRa over most of the Atlantic Ocean (Figures 8a and 8b), the notable exception being the Benguela upwelling region adjacent to the west coast of Southern Africa, which is markedly (up to 5 °C) cooler in HRa. The
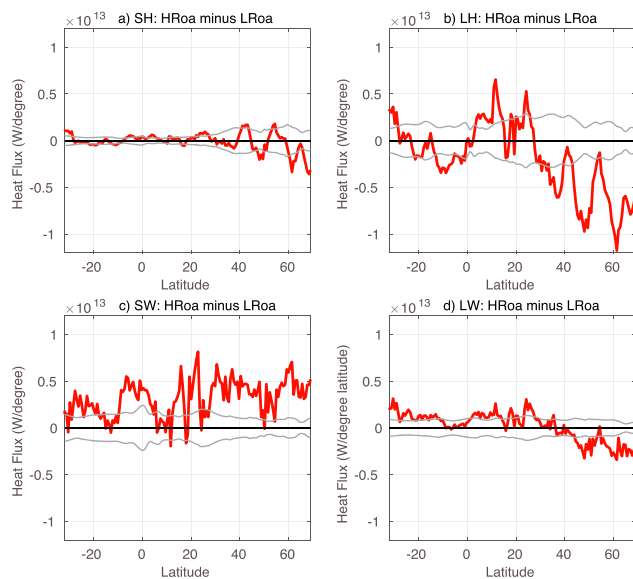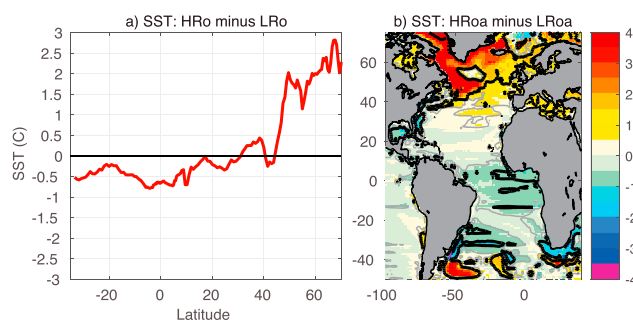

Figure 10. HRoa-LRoa difference in (a) annual mean AOHT (PW) and (b) zonally integrated net surface heat flux for the Atlantic basin (unit: W per degree latitude). AOHT = Atlantic Ocean heat transport.

Figure 11. Annual mean HRoa-LRoa difference in the zonally integrated heat flux components for the Atlantic basin (unit: W per degree latitude): (a) sensible heat flux, (b) latent heat flux, (c) shortwave, and (d) longwave. Gray lines indicate ± the LRoa interannual standard deviation.

increase in North Atlantic SST is consistent with the increase in latent heat flux loss seen in Figure 7b. The HRa-LRa surface air temperature (Figure 9a) has the same sign and a similar spatial pattern to the SST changes implying that the two are strongly coupled. The sign of this change is consistent with an increased SST increasing the heat loss to the lower atmosphere but not with atmospheric temperature driving more heat loss (which would require lower surface air temperatures). There are, however, some indications that the higher-resolution model has stronger wind speeds (Figure 9b). In particular, the increased wind speeds in the Equatorial Atlantic would have led to the stronger latent heat loss there, in the absence of a strong SST increase (Figure 8). There are also significant increases in wind speed in high-latitude regions that may be related to changes in sea ice extent. Finally, there is a widespread reduction in TOA outgoing shortwave radiation (Figure 9c), which equates to a reduction in cloud cover and an increase in the shortwave reaching the Earth's surface. However, the regions where this is significant are mainly equatorial. The region where there is the most significant increase in outgoing TOA shortwave (and a decrease in shortwave reaching the surface) is the Benguela upwelling region. This decrease in surface shortwave is consistent with lower SSTs and latent heat loss. The decreased shortwave at the surface may be associated with an improved representation of the stratocumulus clouds over the upwelling regions arising from the higher-resolution atmosphere. This and other potential causes of this large regional SST bias are the subject of ongoing research (see, e.g., the review by Richter, 2015).

It is noted that this study contains five model integrations where the atmospheric resolution varies between ~100 × 140 km and 25 km but in which the ocean resolution is constant at 1/4°. Tables 2 and 3 show how the heat transport at 26°N and 40°N varies across these model runs. It can be seen, for both 26°N and 40°N, that the 1/4° ocean integrations have a considerable range of AOHT. At 26.5°N, the 1/4° ocean AOHT ranges from 0.92 (±0.08) PW (for HRo 100 × 140-km atmosphere) to 1.20 (±0.14) PW (for LRa 135-km atmosphere) and at 40°N it ranges from 0.60 (±0.06) PW (for LRa 135-km atmosphere) to 0.82 (±0.11) PW (for HRo 100 × 140-km atmosphere). However, the change in AOHT across those five model runs has no correspondence with the change in atmospheric resolution, supporting our conclusions as to the relative insensitivity of AOHT to the resolution of the atmosphere.

Summarizing the changes in the atmosphere-only case, there are evident changes in the shortwave and latent heat components of the surface heat flux. The difference between the atmosphere-only case and the ocean-only case is that these changes are largely balanced locally, eliminating the requirement for significant changes in AOHT. So, for example, in the case of the two resolutions of HadGEM3-GC2.0 runs, resolution-dependent decreases (increases) in cloud cover increase (decrease) the shortwave received at the ocean surface resulting in both higher (lower) SSTs and greater (less) flux of latent heat to the atmosphere.
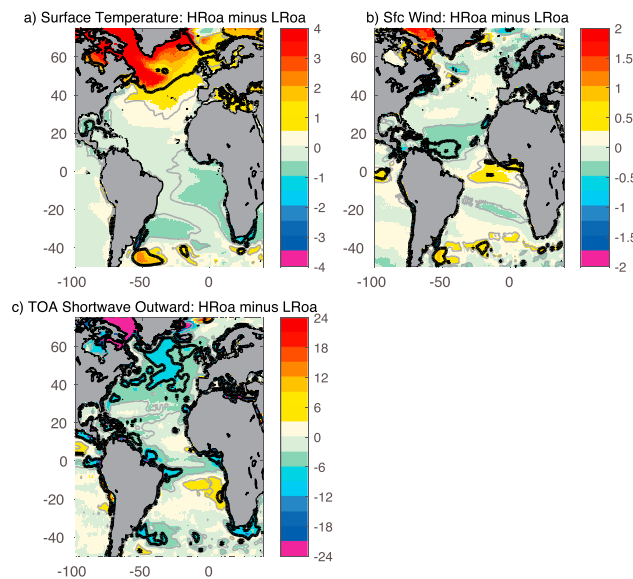
3.3. Experiment 3: Atmosphere and Ocean Resolution Changing

Now we examine the case where both the ocean and atmospheric resolution increase in the EC-Earth model. The mean AOHT for HRoa and LRoa is shown in Figure 1c, and the HRoa-LRoa AOHT difference is shown in Figure 10a. HRoa has increased northward AOHT throughout the Atlantic basin. Between 25°N and 50°N, the difference is greater than 0.2 PW, with two peaks of 0.3 PW difference located at 32°N and 42°N. At the northern end of the basin (65°N) HRoa transport is still greater than LRoa by 0.1 PW. The increase in model AOHT brings it into closer agreement with observations in the North Atlantic subtropics but further away from observations
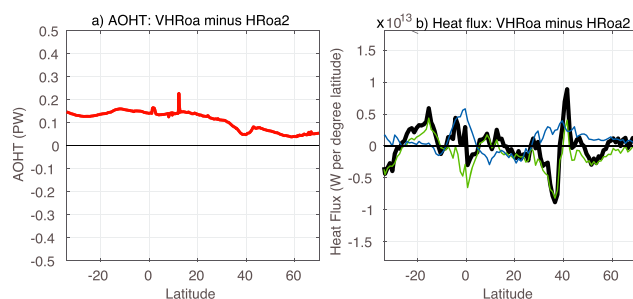

Figure 12. (a) Annual mean HRoa-LRoa difference in zonally integrated SST for the Atlantic basin (°C). Annual mean HRoa-LRoa SST difference (°C). Gray and black contours are one and two standard deviations of LRoa, respectively. SST = sea surface temperature.

Figure 13. Annual mean HRoa-LRoa difference: (a) ocean surface air temperature (°C), (b) ocean surface wind speed (m/s), and (c) TOA outgoing shortwave radiation over the ocean (W/m^2). Gray and black contours are one and two standard deviations of LRoa, respectively. TOA = top of atmosphere.

in the subpolar regions. This result indicates that even with the improvements to AOHT that increased resolution brings, the divergence in AOHT between 26°N and 56°N is still less than implied from hydrographic observations. The implication is also that in this part of the North Atlantic the model is not losing sufficient heat to the atmosphere. We note that this is often the case for a range of surface flux products as well (Grist & Josey, 2003). In the Southern Hemisphere the HRoa-LRoa difference is positive but less than 0.1 PW. To first order, these differences are quite similar to those in the ocean-only case; Figure 2a.

Figure 10b shows HRoa-LRoa zonally integrated net surface heat flux. Broadly speaking, the HRoa-LRoa difference can be divided into two regions. North of 42°N (with the exception of small region near 53°N), where HRoa has enhanced ocean heat loss, and south of 42°N (with the exceptions of small regions at 39°N and 11°S), where HRoa has enhanced ocean heat gain. In order to satisfy energy conservation, in the absence of strong variations in ocean heat storage, the increased tropical-subtropical (0–40°N approximately) heat gain in Figure 10b must be compensated by the increased poleward ocean export of tropical-subtropical heat (Figure 10a). In turn, the decreased heat gain (or increased loss) between 40°N and 60°N is consistent with the poleward decreasing heat transports here. However, the simple pattern of positive at low latitudes and negative at high northern latitudes in the HRoa-LRoa surface heat flux difference is complicated somewhat by short space-scale variability.
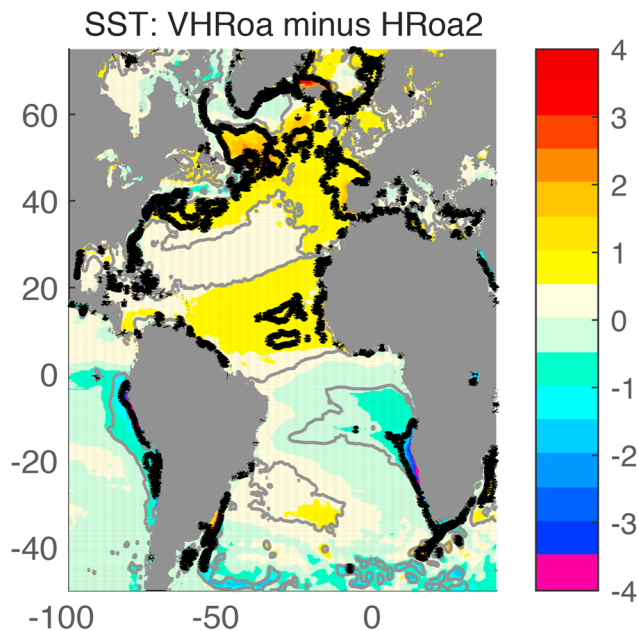
In order to further understand both the broad pattern of southern heat gain/increased northern heat loss in the North Atlantic and the small-scale variability, the changes in the different components of the net heat flux are examined and shown in Figure 11. It is evident that most of the resolution-dependent difference in the net heat flux in the extratropical North Atlantic is primarily associated with changes in the latent heat flux (Figure 11b). This is reinforced by changes in longwave radiation that are about one third of the size of the latent heat changes but acting in the same sense. In the North Atlantic, the increased heat loss from latent heat and longwave is partially compensated by a large increase in incoming shortwave radiation. Over most of the length of the basin, there are increases in incoming shortwave, with consistently large increases occurring north of 30°N. This is similar to the atmosphere-only case (Figure 7) but does not agree well with the ocean-only case (Figure 3).

Summarizing the atmosphere-ocean case to this point, it is noted first that there is a significant increase in AOHT, which is higher particularly between 20°N and 42°N, before decreasing further to the north and that this is balanced by increases in surface net heat flux into (out of) the ocean to the south (north) of 42°N. Further, the changes in net flux are primarily made up of increased ocean heat loss via latent heat and longwave in the subpolar gyre and increased shortwave flux into the ocean over the length of the basin.

Having established the nature of the changes in ocean heat transport and surface heat flux changes for the ocean-atmosphere case, we now examine changes in surface fields that may be associated with these changes. The zonally integrated HRoa-LRoa SST difference is plotted in Figure 12a. It shows an increase in SST with resolution (>1 °C and typically 2 °C) north of 44°N. The higher SST is consistent with ocean changes driving increased latent, sensible, and longwave loss to the atmosphere. These changes to SST are similar to (but stronger than) those in the ocean-only case in Figure 4 (HRo minus LRo). As was the case with HRo minus LRo, the spatial pattern of SST increase (Figure 12b) in the North Atlantic includes the region adjacent to the Labrador and Greenland Coast, likely related to a reduction in sea ice, and a region further to the east (50°N, 20°W) consistent with a stronger eastward extension of the North Atlantic Current.

Figure 14. VHRoa-HRoa2 difference in (a) annual mean AOHT (PW) and (b) zonally integrated net surface heat flux (black line), latent heat flux (green line), and shortwave flux (blue line) for the Atlantic basin (unit: W per degree latitude). AOHT = Atlantic Ocean heat transport.

Figure 15. Annual mean VHRoa-HRoa2 SST (°C) difference. Gray and black contours are one and two standard deviations of HRoa2, respectively. SST = sea surface temperature.

Confirmation that the large HRoa-LRoa change in North Atlantic surface fluxes was not primarily instigated by atmospheric changes is now presented. Specifically, Figure 13a shows that the large positive SST anomalies are accompanied by positive surface air temperature anomalies. This change in air temperature is in the opposite sense to that which would promote the enhanced latent and longwave loss seen in Figures 11b and 11d. Similarly, there are no changes in the wind speed in the region (Figure 13b) that would have promoted an increase in heat loss from the sensible or latent heat terms (Figures 11a and 11b). This is a similar situation to the ocean-only case (Figure 5b). In the tropics, however, there is a significant decrease in the surface wind. Specifically, in the western half of the Atlantic between 10°N and 20°N, a decrease in wind speed could have supported the reduction in latent heat loss at these latitudes seen in Figure 11b.

The final atmospheric field that we consider changes in is the cloud cover. As a proxy for this we use the TOA outgoing shortwave radiation, since high values indicate more clouds reflecting shortwave and low values more shortwave reaching the surface through reduced cloud cover (Figure 13c). The most significant difference is a reduction in cloud cover in the subpolar gyre and in Baffin Bay, although the reduction is evident over most of the basin. Again, this is consistent with the increase in shortwave radiation noted over most of the basin in Figure 11c.

To summarize the changes associated with moving from LRoa to HRoa, it is evident that there is a significant increase in northward ocean heat transport in the North Atlantic. This is balanced primarily by an increase in mid-high latitude latent heat loss. The increased latent heat loss is associated with increased SSTs (and probably reduced sea-ice coverage) and is driven by the ocean resolution change as opposed the atmospheric resolution change (i.e., since it would require a decreased surface air temperature/specific humidity for the atmosphere to promote increased latent and sensible heat flux rather than the increased surface temperature in Figure 13a). The increased atmospheric resolution was associated, however, with a reduction in cloud cover and increased incoming solar radiation which partially compensated the increased latent heat loss.

4. Experiment 4: CMIP6 Models, Increasing the Resolution to 1/12° Ocean and 25-km Atmosphere

Thus far, we have considered changes accompanying (ocean) model resolution increases from ~1° to 1/4°, with an atmosphere resolution of up to 25 km. We now briefly examine the change in AOHT that occurs with a change of resolution that may be typical of future/CMIP6 climate models. Specifically, we compare the *High Resolution (HRoa2)* HadGEM3 GC2.1 with an N216 atmosphere and the 1/4° eddy-permitting (ORCA025) ocean with the *Very High Resolution (VHRoa)* version with the N512 atmosphere and 1/12° eddy-resolving ocean model (ORCA12). The AOHT simulated in HRoa2 and VHRoa is shown in Figure 1d with the difference shown in Figure 14a. In these panels the cyan crosses indicate latitudes for which there is a significant difference between VHRoa and HRoa2 (specifically, where the model AOHT values do not fall within each other's standard deviations). It is clear that, in the case of this model, moving to a climate model with an ocean eddy-resolving resolution results in another step change improvement in the representation of the AOHT. However, the latitude band of the most significant changes is further south compared to the HRo-LRo and HRoa-LRoa cases. The VHRoa-HRoa2 difference is greater than 0.1 PW south of 30°N, and the change is significant between 10°S and 2°N. There are also significant differences at 12°N and between 63°N and 70°N. The AOHT changes at low latitudes are in the sense to bring the modeled AOHT more in line with observations, whereas although the significant high-latitude changes are just to the north of the hydrographic estimate at 56°N, the changes at 56°N tend to take the model estimates further away from these observations.

A consequence of the most significant change in AOHT being further south than in HRoa-LRoa and HRo-LRo is that the increase in zonally integrated net heat loss to the atmosphere is also further to the south. Whereas
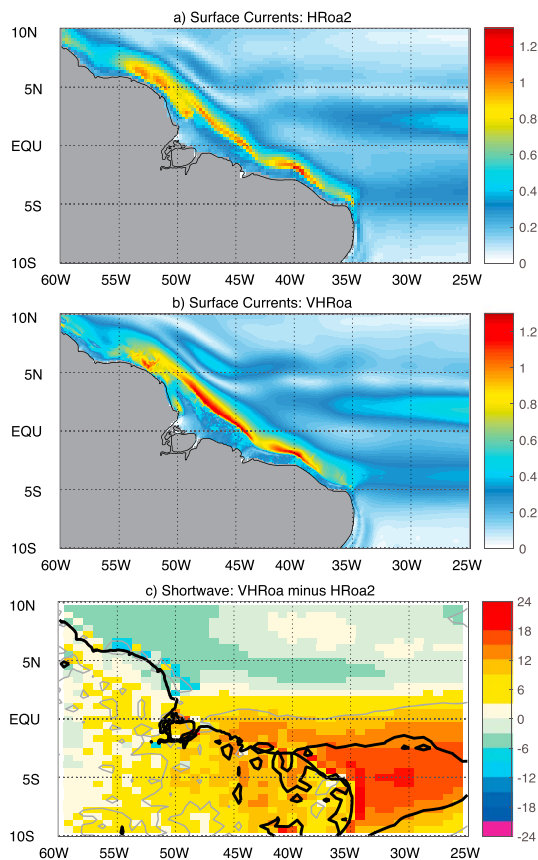
Figure 16. Equatorial tropical Atlantic surface current speed in (a) HRoa2 and (b) VHRoa (unit: m/s). (c) VHRoa-HRoa2 shortwave flux (W/m^2). Gray and black contours are one and two standard deviations of HRoa2, respectively.

for HRoa-LRoa and HRo-LRo, the increased net heat loss mostly occurs north of 40°N, for VHRoa-HRoa2 the increase in heat loss occurs between 15°N and 58°N except between 40°N and 50°N where ocean heat gain increases (Figure 14b). Most of the increased heat loss is again associated with increased latent heat loss (see green line in Figure 14b). The low latitude and southern Atlantic heat gain is associated with decreased latent heat loss between 25°S and 10°S and 5°N and 12°N, and increased shortwave flux between 10°S and 4°N (blue line in Figure 14b).

As discussed in Roberts et al. (2016) and Hewitt et al. (2016), the greater North Atlantic oceanic latent heat release in VHRoa is associated with improved representation of SSTs. The VHRoa-HRoa2 SST field in Figure 15 shows the higher resolution that leads to higher temperatures in much of the North Atlantic. Hewitt et al. (2016) noted that SST changes are linked to a change in the location of the NAC associated with increased ocean resolution. In addition, here we point out that significant increases in latent heat loss occur to the south of the NAC and that these are balanced by more heat being transported from the tropics. Figure 16 compares the surface ocean currents in the tropical Atlantic in VHRoa and HRoa2. It is evident that the mean VHRoa current speed is much stronger in the predominantly northward boundary currents such as the North Brazil Current. The stronger mean currents afforded by the eddy-resolving ocean would partially facilitate the stronger AOHT and North Atlantic heat loss. However, this is also promoted by a stronger influx of shortwave radiation (Figure 16c) and higher SSTs (Figure 15) in the western tropical Atlantic. This is consistent with the analysis of the same models by Roberts et al. (2016). They found that the difference in AOHT between eddy-permitting and eddy-resolving resolutions was mainly due to the change in mean temperatures and currents as opposed to the time-varying component.

Summarizing the case of VHRoa-HRoa2, we note that the changes fit the pattern of HRoa-LRoa and HRo-LRo in that the northward ocean heat transport increases significantly and that this is balanced by increased ocean heat loss to the north and heat gain to the south. A further similarity is that the increased northern heat loss is facilitated by elevated SSTs enhancing latent heat loss. A key difference is that in moving to the eddy-resolving ocean these changes occur further south. The implication of this from our analysis and the work of Roberts et al. (2016) is that for this change in model resolution, this is where the greater changes in the mean ocean circulation occur.

5. Conclusions

In conclusion, the results for the three models considered in our main analysis reveal that the resolution of the ocean component is the key factor for increasing the ocean heat transfer in the Atlantic. In Experiment 1, the increase in ocean resolution from 1° (non eddy resolving) to 1/4° (eddy resolving) strengthens AOHT, bringing about 30% more heat to the mid-high latitude North Atlantic. In turn this increases the mid-high-latitude SST and latent heat loss. In contrast, increasing the resolution of the atmospheric component in Experiment 2 from 130 to 25 km in Experiment 2 has little, if any, impact on the strength of the heat transport. It does lead to strong regional changes in the shortwave input to the ocean as a result of decreasing cloud cover, but these are locally balanced by increased latent heat loss. Consequently the AOHT does not change significantly. When the resolution of both components is increased in Experiment 3, the changes in the ocean circulation dominate and the AOHT increase is similar to that found when only the ocean resolution changes (Experiment 1). Although we have only been able to explore comparisons between three models at length, and we note the caveat that the length of the high-resolution simulations, in particular, means that the influence of model drift cannot be completely removed, we present this as a paradigm for understanding resolution-dependent changes in ocean heat transport across a broad spectrum of coupled models.

The model values of AOHT have here been evaluated against a limited number of individual direct hydrographic estimates. In addition to this, since 2004, the RAPID array at 26°N, designed for continuously observing the strength of the AMOC, has also been used to estimate the northward ocean heat transport (Johns et al., 2011) as 1.3 (±0.4) PW. A benefit of the RAPID array is that it is near the latitude of maximum northward transport. Based on this measure at the most observed latitude, the increase in AOHT associated with the change from non eddy-resolving to eddy-resolving ocean brings the AOHT more in line with observations. It is expected that the new OSNAP array at 52–60°N (see Lozier et al., 2017), together with the RAPID array, will provide robust estimates of the North Atlantic heat transport convergence between these latitudes against which to evaluate future climate models.

Finally, a preliminary examination of HadGEM3 2.1, comparing models with oceans at 1/4° and 1/12° resolutions, suggests that the framework for understanding resolution changes may hold as climate models move toward resolutions which may be more typical for future exercises such as CMIP7. In particular, the finer resolution produces a further significant rise in AOHT, likely due to strengthening currents, and is accompanied by a compensating increased net ocean heat gain (from the atmosphere) to the south and increased heat loss to the north.

In general, this research has revealed that as climate models increase their resolution, both from 1° to 1/4° and from 1/4° to 1/12°, the AOHT increases significantly. These changes bring the models into greater agreement with existing observational estimates in the equatorial and subtropical regions. In subpolar regions, the increase moves the AOHT estimates further away from the observations although the full significance of this will only become clear once reliable continuous measurements are available from OSNAP. A potential implication is that model ocean heat transport divergence or heat loss to the atmosphere in the midlatitude North Atlantic remains too weak in the climate models. Further research on this issue is timely as the estimates of AOHT from RAPID and OSNAP, combined with Argo profiling float measurements, should enable more robust estimates of midlatitude heat transport divergence in the near future.

References

Bryden, H. L., & Hall, M. M. (1980). Heat transport by currents across 25°N latitude in the Atlantic Ocean. *Science*, *207*(4433), 884–886. https://doi.org/10.1126/science.207.4433.884

Bryden, H. L., Longworth, H. R., & Cunningham, S. A. (2005). Slowing of the Atlantic meridional overturning circulation at 25°N. *Nature*, *438*, 655–657.

Buchan, J., Hirschi, J. J.-M., Blaker, A. T., & Sinha, B. (2014). North Atlantic SST anomalies and the cold north European weather events of winter 2009-10 and December 2010. *Monthly Weather Review*, *142*(2), 922–932. https://doi.org/10.1175/MWR-D-13-00104.1

Cunningham, S. A., Kanzow, T., Rayner, D., Baringer, M. O., Johns, W. E., Marotzke, J., et al. (2007). Temporal variability of the Atlantic meridional overturning circulation at 25°N. *Science*, *317*(5840), 935–938. https://doi.org/10.1126/science.1141304

Fogli, P. G., & Iovino, D. (2014). CMCC-CESM-NEMO: Toward the new CMCC Earth System Model. CMCC Research Paper No. 248. Retrieved from http://www.cmcc.it/wp-content/uploads/2015/02/rp0248-ans-12-2014.pdf

Grist, J. P., & Josey, S. A. (2003). Inverse analysis adjustment of the SOC air–sea flux climatology using ocean heat transport constraints. *Journal of Climate*, *16*(20), 3274–3295. https://doi.org/10.1175/1520-0442(2003)016<3274:IAAOTS>2.0.CO;2

Grist, J. P., Josey, S. A., Jacobs, Z. L., Marsh, R., Sinha, B., & Van Sebille, E. (2016). Extreme air–sea interaction over the North Atlantic subpolar gyre during the winter of 2013–2014 and its sub-surface legacy. *Climate Dynamics*, *46*(11-12), 4027–4045. https://doi.org/10.1007/s00382-015-2819-3

Grist, J. P., Josey, S. A., Marsh, R., Good, S. A., Coward, A. C., de Cuevas, B. A., et al. (2010). The roles of surface heat flux and ocean heat transport convergence in determining Atlantic Ocean temperature variability. *Ocean Dynamics*, *60*(4), 771–790. https://doi.org/10.1007/s10236-010-0292-4

Haarsma, R., Roberts, M., Vidale, P. L., Senior, C., Bellucci, A., Corti, S., et al. (2016). High Resolution Model Intercomparison Project (HighResMIP). *Geoscientific Model Development*, *9*, 4185–4208. www.geosci-model-dev.net/9/4185/2016/doi:10.5194/gmd-9-4185-2016gmd-2016-66

Hazeleger, W., Wang, X., Severijns, C., Stefanescu, S., Bintanja, R., Sterl, A., Wyser, K., et al. (2012). EC-EarthV2: Description and validation of a new seamless Earth system prediction model. *Climate Dynamics*, *39*(11), 2611–2629. https://doi.org/10.1007/s00382-011-1228-5

Hewitt, H. T., Roberts, M. J., Hyder, P., Graham, T., Rae, J., Belcher, S. E., et al. (2016). The impact of resolving the Rossby radius at mid-latitudes in the ocean: Results from a high-resolution version of the Met Office GC2 coupled model. *Geoscientific Model Development*, *9*(10), 3655–3670. https://doi.org/10.5194/gmd-9-3655-2016

Hobbs, W. R., & Willis, J. K. (2012). Midlatitude North Atlantic heat transport: A time series based on satellite and drifter data. *Journal of Geophysical Research*, *117*, C01008. https://doi.org/10.1029/2011JC007039

Holfort, J., & Siedler, G. (2001). The meridional oceanic transports of heat and nutrients in the South Atlantic. *Journal of Physical Oceanography*, *31*(1), 5–29. https://doi.org/10.1175/1520-0485(2001)031<0005:TMOTOH>2.0.CO;2

Holliday, N. P., Bacon, S., Cunningham, S. A., Gary, S. F., Karstensen, J., King, B. A., et al. (2018). Subpolar North Atlantic overturning and gyre-scale circulation in the summers of 2014 and 2016. *Journal of Geophysical Research: Oceans*, *123*, 4538–4559. https://doi.org/10.1029/2018JC013841

Ingleby, B., & Huddleston, M. R. (2007). Quality control of ocean temperature and salinity profiles—Historical and real-time data. *Journal of Marine Systems*, *65*(1-4), 158–175. https://doi.org/10.1016/j.jmarsys.2005.11.019

Jia, Y. (2003). Ocean heat transport and its relationship to ocean circulation in the CMIP coupled models. *Climate Dynamics*, *20*(2), 153–174. https://doi.org/10.1007/s00382-002-0261-9

Johns, W. E., Baringer, M. O., Beal, L. M., Cunningham, S. A., Kanzow, T., Bryden, H. L., et al. (2011). Continuous, array-based estimates of Atlantic Ocean heat transport at 26.5°N. *Journal of Climate*, *24*(10), 2429–2449. https://doi.org/10.1175/2010JCLI3997.1

Josey, S. A., Hirschi, J. J.-M., Sinha, B., Duchez, A., Grist, J. P., & Marsh, R. (2018). The recent Atlantic cold anomaly: Causes, consequences, and related phenomena. *Annual Review of Marine Science*, *10*(1), 475–501. https://doi.org/10.1146/annurev-marine-121916-063102

Kanzow, T., Cunningham, S. A., Johns, W. E., Hirschi, J. J.-M., Marotzke, J., Baringer, M. O., et al. (2010). Seasonal variability of the Atlantic meridional overturning circulation at 26.5°N. *Journal of Climate*, *23*(21), 5678–5698. https://doi.org/10.1175/2010JCLI3389.1

Kirtman, B. P., Bitz, C., Bryan, F., Collins, W., Dennis, J., Hearn, N., et al. (2012). Impact of ocean model resolution on CCSM climate simulations. *Climate Dynamics*, *39*(6), 1303–1328. https://doi.org/10.1007/s00382-012-1500-3

Klein, B., Molinari, R. L., Mueller, T. J., & Siedler, G. (1995). A transatlantic section at 14.5 N: Meridional volume and heat fluxes. *Journal of Marine Research*, *53*(6), 929–957. https://doi.org/10.1357/0022240953212963

Koenigk, T., & Brodeau, L. (2017). Arctic climate and its interaction with lower latitudes under different levels of anthropogenic warming in a global coupled climate model. *Climate Dynamics*, *49*(1–2), 471–492. https://doi.org/10.1007/s00382-016-3354-6

Lavin, A., Bryden, H. L., & Parrilla, G. (1998). Meridional transport and heat flux variations in the subtropical North Atlantic. *The Global Atmosphere and Ocean System*, *6*, 269–293.

Lozier, M. S., Femke de Jong, M., de Steur, L., de Young, B., Fischer, J., Gary, S. F., et al. (2017). Overturning in the subpolar North Atlantic program: A new international ocean observing system. *Bulletin of the American Meteorological Society*, *98*(4), 737–752. https://doi.org/10.1175/BAMS-D-16-0057.1

Madec, G. (2008). Note du Pôle de modélisation, Institut Pierre-Simon Laplace (IPSL), France, No 27.

Maidens, A., Arribas, A., Scaife, A. A., MacLachlan, C., Peterson, D., & Knight, J. (2013). The influence of surface forcings on the North Atlantic oscillation regime of winter 2010/11. *Monthly Weather Review*, *141*, 3801–3813. https://doi.org/10.1175/MWR-D-13-00033.1

McCarthy, G. D., Smeed, D. A., Johns, W. E., Frajka-Williams, E., Moat, B. I., Rayner, D., Baringer, M. O., et al. (2015). Measuring the Atlantic meridional overturning circulation at 26°N. *Progress in Oceanography*, *130*, 91–111. https://doi.org/10.1016/j.pocean.2014.10.006

Msadek, R., Johns, W. E., Yeager, S. G., Danabasoglu, G., Delworth, T., & Rosati, T. (2013). The Atlantic meridional heat transport at 26.5°N and its relationship with the MOC in the RAPID-array and GFDL and NCAR coupled models. *Journal of Climate*, *26*, 4335–4356. https://doi.org/10.1175/JCLI-D-12-0008.1

Pohlmann, H., Sienz, F., & Latif, M. (2006). Influence of the multidecadal Atlantic meridional overturning circulation variability on European climate. *Journal of Climate*, *19*(23), 6062–6067. https://doi.org/10.1175/JCLI3941.1

Richter, I. (2015). Climate model biases in the eastern tropical oceans: Causes, impacts and ways forward. *WIREs Climate Change*, *6*(3), 345–358. https://doi.org/10.1002/wcc.338

Roberts, M. J., Hewitt, H. T., Hyder, P., Ferreira, D., Josey, S. A., Mizielinski, M., & Shelly, A. (2016). Impact of ocean resolution on coupled air-sea fluxes and large-scale climate. *Geophysical Research Letters*, *43*, 10,430–10,438. https://doi.org/10.1002/2016GL070559

Speer, K., Holfort, G. J., Reynaud, T., & Siedler, G. (1996). South Atlantic heat transport at 11S. In *The South Atlantic: Present and past circulation* (pp. 105–120). Berlin: Springer.

Sterl, A., Bintanja, R., Brodeau, L., Gleeson, E., Koenigk, T., Schmith, T., et al. (2012). A look at the ocean in the EC-Earth climate model. *Climate Dynamics*, *39*(11), 2631–2657. https://doi.org/10.1007/s00382-011-1239-2

Sutton, R. T., & Hodson, D. L. R. (2005). Atlantic ocean FORCING of North American and European summer climate. *Science*, *309*(5731), 115–118. https://doi.org/10.1126/science.1109496

Trenberth, K. E., & Caron, J. M. (2001). Estimates of meridional atmosphere and ocean heat transports. *Journal of Climate*, *14*(16), 3433–3443. https://doi.org/10.1175/1520-0442(2001)014<3433:EOMAAO>2.0.CO;2

Trenberth, K. E., & Fasullo, J. T. (2017). Atlantic meridional heat transports computed from balancing Earth's energy locally. *Geophysical Research Letters*, *44*, 1919–1927. https://doi.org/10.1002/2016GL072475

Williams, K. D., Copsey, D., Blockley, E. W., Bodas-Salcedo, A., Calvert, D., Comer, R., et al. (2017). The Met Office Global Coupled model 3.0 and 3.1 (GC3.0 and GC3.1) configurations. *Journal of Advances in Modeling Earth Systems*, *10*, 357–380. https://doi.org/10.1002/2017MS001115

Williams, K. D., Harris, C. M., Bodas-Salcedo, A., Camp, J., Comer, R. E., Copsey, D., et al. (2015). The Met office global coupled model 2.0 (GC2) configuration. *Geoscientific Model Development*, *8*(5), 1509–1524. https://doi.org/10.5194/gmd-8-1509-2015